BBA - Biomembranes 1867 (2025) 184404

Contents lists available at ScienceDirect

BBA - Biomembranes

journal homepage: www.elsevier.com/locate/bbamem

Characterization of intact FeoB in a lipid bilayer using styrene-maleic acid (SMA) copolymers

Mark Lee, Candice M. Armstrong, Aaron T. Smith *

Department of Chemistry and Biochemistry, University of Maryland, Baltimore County, Baltimore, MD 21250, USA

ARTICLE INFO

Keywords:
Feo
iron
SMALP
transport
mass photometry

ABSTRACT

The acquisition of ferrous iron (Fe^{2+}) is crucial for the survival of many pathogenic bacteria living within acidic and/or anoxic conditions such as *Vibrio cholerae*, the causative agent of the disease cholera. Bacterial pathogens utilize iron as a cofactor to drive essential metabolic processes, and the primary prokaryotic Fe^{2+} acquisition mechanism is the ferrous iron transport (Feo) system. In *V. cholerae*, the Feo system comprises two cytosolic proteins (FeoA, FeoC) and a complex, polytopic transmembrane protein (FeoB) that is regulated by an N-terminal soluble domain (NFeoB) with promiscuous NTPase activity. While the soluble components of the Feo system have been frequently studied, very few reports exist on the intact membrane protein FeoB. Moreover, FeoB has been characterize almost exclusively in detergent micelles that can cause protein misfolding, disrupt protein oligomerization, and even dramatically alter protein function. As many of these characteristics of FeoB remain unclear, there is a critical need to characterize FeoB in a more native-like lipid environment. To address this unmet need, we employ styrene-maleic acid (SMA) copolymers to isolate and to characterize *V. cholerae* FeoB (*Vc*FeoB) encapsulated by a styrene-maleic acid lipid particle (SMALP). In this work, we describe the development of a workflow for the expression and the purification of *Vc*FeoB in a SMALP. Leveraging mass photometry, we explore the oligomerization of FeoB in a lipid bilayer and show that the *Vc*FeoB-SMALP is mostly monomeric, consistent with our previous oligomerization observations *in surfo*. Finally, we characterize the NTPase activity of *Vc*FeoB in the SMALP and in a detergent (DDM), revealing higher NTPase activity in the presence of the lipid bilayer. When taken together, this report represents the first characterization of any FeoB in a native-like lipid bilayer and provides a viable approach for the future structural characterization of FeoB.

1. Introduction

The acquisition of iron is an essential process for the growth and virulence of virtually all pathogenic bacteria [1–3]. During infection, the iron obtained directly from the host is incorporated into a diverse set of proteins that utilize this element as an important cofactor for catalysis, such as with *de novo* DNA biosynthesis, electron transport, and even N_2 fixation [4–6]. Given the critical nature of iron to bacterial fitness, these pathogens have evolved to utilize numerous strategies to acquire this important nutrient, and these strategies are generally dependent on both the chelation status and the oxidation state of the iron ion. To solubilize the extremely insoluble ferric iron (Fe^{3+}), bacteria commonly deploy siderophores that can scavenge the environment for Fe^{3+} ions from small molecule complexes or even directly from ferritin or transferrin [7–10]. Additionally, bacteria can also produce hemophores and outer membrane receptors that directly sequester iron protoporphyrin IX (heme *b*) from host hemoproteins [11–14]. Both Fe^{3+}-bound siderophores and heme may be brought into the cytoplasm through the use of ATP binding cassette (ABC) transporters, or the iron may be released by reductive dissociation catalyzed *via* ferric reductases or heme oxygenases [15,16]. While the acquisition of Fe^{3+} and heme are both prevalent at the host-pathogen interface under oxic conditions, the

Abbreviations: ATP, adenosine triphosphate; CMC, critical micellular concentration; cryo-EM, cryogenic electron microscopy; DDM, *n*-dodecyl-β-D-maltoside; FeoB, ferrous iron transport protein B; FPLC, fast protein liquid chromatography; GDN, glycol-diosgenin; GTP, guanosine triphosphate; IMAC, immobilized metal affinity chromatography; IPTG, isopropyl β-D-1-thiogalactopyranoside; LMNG, lauryl maltose neopentyl glycol; MP, mass photometry; MSP, membrane scaffold protein; NFeoB, N-terminal domain of FeoB; NTP, nucleotide triphosphate; SDS-PAGE, sodium dodecyl-sulfate polyacrylamide gel electrophoresis; SEC, size-exclusion chromatography; SMA, styrene maleic-acid; SMALP, styrene maleic-acid lipid particle; SUMO, small ubiquitin-like modifier; TEV, tobacco etch virus.

* Corresponding author.
E-mail address: smitha@umbc.edu (A.T. Smith).

https://doi.org/10.1016/j.bbamem.2024.184404
Received 20 August 2024; Received in revised form 12 November 2024; Accepted 12 December 2024
Available online 16 December 2024

acquisition of ferrous iron (Fe^{2+}) is important at the host-pathogen interface in acidic and/or anoxic environments, such as those encountered within the stomach or the gastrointestinal tracts of humans [17,18].

To accomplish Fe^{2+} acquisition, pathogenic bacteria rely chiefly on the ferrous iron transport (Feo) system, the most widely distributed and dedicated Fe^{2+} transporter found across the prokaryotic domain [18–21]. The Feo system is generally considered an important virulence factor present in virtually all clinically-relevant Gram-negative γ-proteobacteria, such as *Vibrio cholerae*, the causative agent of the disease cholera. In these pathogens, Feo comprises three proteins, two of which are cytosolic (FeoA and FeoC), and one of which is a complex, polytopic membrane protein (FeoB) consisting of a soluble N-terminal domain tethered to a large α-helical transmembrane domain responsible for the transport of Fe^{2+} (Fig. 1). FeoA is a small SH3-like protein that has been shown to interact with FeoB in a number of bacterial species (including *V. cholerae*) both *in vitro* and *in vivo* [22,23], and FeoA is currently hypothesized to stabilized the NTP-bound form of FeoB to keep the Fe^{2+}-permeable protein channel open [23]. Similarly, FeoC has been shown to interact with FeoB both *in vitro* and *in vivo* (including in *V. cholerae*) [24–26], but the function of FeoC remains more elusive than FeoA due to its large sequence diversity and poor conservation. While all structurally characterized FeoCs have a winged-helix motif [26], and many FeoC proteins bind [4Fe-4S] clusters *via* a Cys-rich motif in their unstructured wing regions [27], FeoC proteins in the *Vibrio* genus of bacteria do not contain any identifiable metal-binding motifs [26], and their function remains unclear. It has been hypothesized that all three proteins interact together to form a competent transport complex

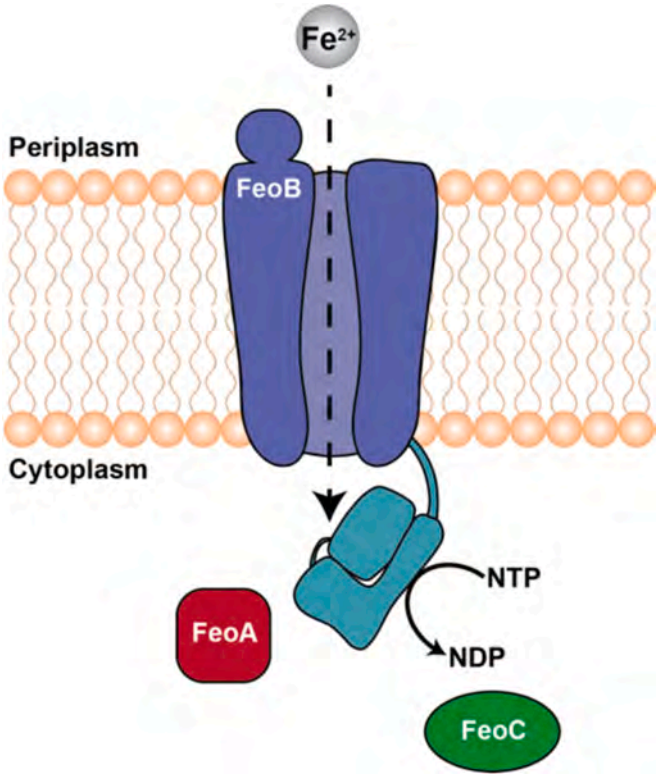

Fig. 1. Cartoon overview of the Feo system present in a Gram-negative γ-proteobacterium such as *Vibrio cholerae*. In most Gram-negative γ-proteobacteria, the Feo system consists of three proteins: two cytosolic proteins known as FeoA (red) and FeoC (green), and a large polytopic transmembrane protein known as FeoB (purple). In *V. cholerae*, FeoB contains a large soluble N-terminal domain (NFeoB, teal) that is postulated to use NTPase activity to open and to close a channel that facilitates the transport of ferrous iron (Fe^{2+}, gray sphere) into the cytoplasmic space. (For interpretation of the references to colour in this figure legend, the reader is referred to the web version of this article.)

[25,28,29], but the majority of *feo* operons lack the FeoC protein, and an FeoA-FeoB-FeoC multiprotein complex has not been structurally or biophysically characterized.

A major impasse in the Feo field remains to be the lack of a structure of intact FeoB, the most important and wholly conserved protein of the Feo system. In contrast to intact FeoB, several structures exist of the N-terminal soluble G-protein-like domain of FeoB (NFeoB) in its nucleotide-free and nucleotide-bound forms [30–38], including very recent reports of apo and nucleotide-bound *V. cholerae* NFeoB [39]. These structures have revealed that NFeoB has structural homology to eukaryotic G-proteins, but how the binding of nucleotide in this domain is related to the translocation of Fe^{2+} remains unclear. In fact, only recently have reports have demonstrated that intact and active FeoB can be expressed, purified, and isolated in detergent micelles to homogeneity [40,41]. However, as this momentum shifts and FeoB becomes more readily available from recombinant systems, the possibility of an intact FeoB structure may be a future reality, if suitable samples can be prepared for structural approaches such as cryo-EM.

As cryo-EM advances as a structural technique and becomes more and more accessible, several approaches to solving structures of membrane proteins exist that could be leveraged for FeoB structural determination now that FeoB can be expressed and purified. Since 2014, the number of membrane protein structures determined per year has risen due to improvements and advances in cryo-EM technology and, in 2018, cryo-EM determined structures exceeded the number of structures per year determined by X-ray crystallography [42,43]. However, a major bottleneck in cryo-EM structural determination remains membrane protein sample preparation [44]. One logical first approach is the use of non-denaturing detergents to solubilize the hydrophobic portion of membrane proteins due to their instability outside of a lipid bilayer (Fig. 2); however, empty detergent micelles have been known to interfere with the particle picking data processing, as micelles can be difficult to differentiate especially from small membrane protein (molecular weight < 100 kDa) [45]. The development of detergents such as glycol-diosgenin (GDN) and lauryl maltose neopentyl glycol (LMNG) has helped, as these detergents have very low critical micellular concentrations (CMCs), but issues still occur, such as the disruption of oligomerization, the loss of lipids, and even inactivation of enzymes [46].

Alternatively, to circumvent the negative effects of detergents on membrane protein structure and function, membrane mimetic systems have been used to mimic the lipid bilayer more closely. The initial model for a membrane mimetic system was developed by utilizing a membrane scaffold protein (MSP) derived from human apolipoprotein that encapsulates membrane proteins into a lipid bilayer wrapped with the MSP (Fig. 2) [47]. However, this method is dependent upon first solubilizing the membrane protein with detergents, then introducing detergent/lipid micelles, followed by detergent removal (either by polystyrene beads or prolonged dialysis) to promote the formation of a lipid bilayer, and finally encapsulation of the complex by the MSP [48]. Although the MSP-nanodisc technique has been very successful, detergent solubilization is still required, which could destabilize or inactivate the membrane protein during sample preparation. Alternatively, detergent-free alternatives to MSP nanodiscs have emerged as viable methods to purify membrane proteins directly from the lipid bilayer for protein structural determination [49]. One newer approach is the use of styrene-maleic acid (SMA) copolymers, an organic copolymer that is able to sequester membrane proteins directly from cell membranes by formation of a styrene-maleic acid lipid particle (SMALP) (Fig. 2) [50]. SMA-copolymers have recently been used to solve cryo-EM structures of membrane proteins surrounded by native-like lipids without exposure to detergents [51,52]. While there are some disadvantages of SMALPs, like their propensity to chelate various metal ions [53–56], the lack of a detergent solubilization step and the ability to incorporate native lipids are major assets of this recently-developed approach.

In this work, we explore the use of styrene-maleic acid copolymers to purify intact *V. cholerae* FeoB (*Vc*FeoB) in a detergent-free manner. To

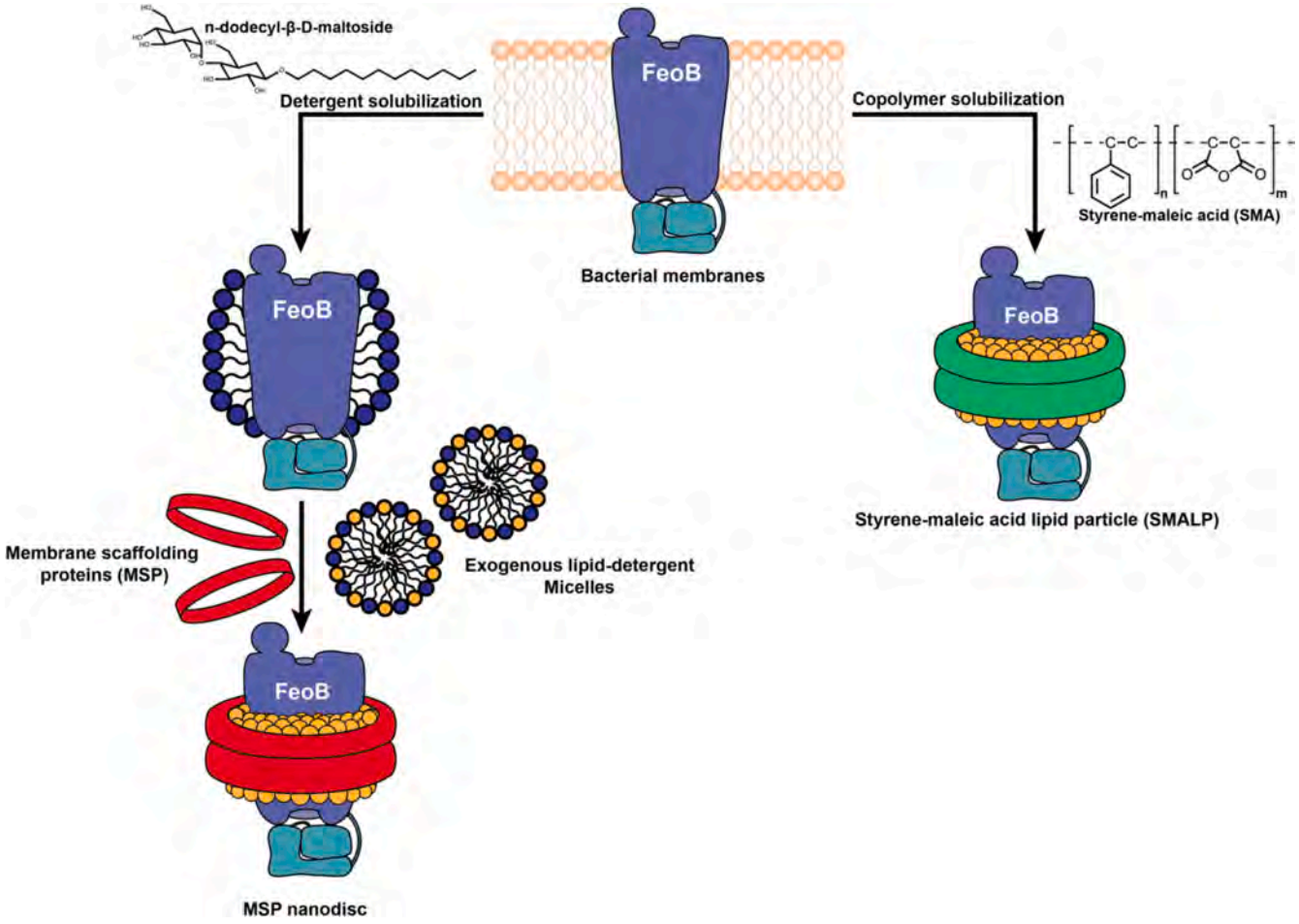

Fig. 2. Membrane proteins can be extracted from lipid bilayers in multiple ways. The first and most traditional way is *via* solubilization with a non-denaturing detergent such as DDM. The detergent-solubilized membrane protein can then be reintroduced into a lipid bilayer by utilizing membrane scaffolding proteins (MSP) and exogenous lipid-detergent micelles. Removal of detergent promotes the formation of a lipid bilayer and encapsulation by the MSP. Alternatively, membrane proteins can be extracted directly from the native lipid bilayer by the addition of styrene-maleic acid (SMA) copolymers that sequester membrane proteins and lipids directly from the lipid bilayer, leading to a more native-like environment known as the styrene-maleic acid lipid particle (SMALP).

do so, we tested multiple different *Vc*FeoB expression constructs and found the optimal method of SMALP-based extraction occurred using the SMA200 system coupled to a C-terminally $(Strep)_2$-tagged *Vc*FeoB protein. Once purified, we used mass photometry to characterize the size distribution of the *Vc*FeoB-SMALP complex, which is most consistent with a single FeoB polypeptide embedded within a lipid bilayer. Finally, we compared the rates of ATP and GTP hydrolysis between detergent-solubilized *Vc*FeoB and SMALP-encapsulated *Vc*FeoB and found increases in the hydrolytic rates of both nucleotide triphosphates when *Vc*FeoB was present within the SMALP. To our knowledge, this report represents the first example of FeoB prepared in a detergent-free manner, and this approach may facilitate future structural studies of intact FeoB.

2. Results

2.1. Initial attempts to purify $(His)_6$-tagged VcFeoB using SMALPs

We initially attempted to purify in a detergent-free manner C-terminally $(His)_6$-tagged *Vc*FeoB (*Vc*FeoB-$(His)_6$; *ca.* 85 kDa), a construct that was previously designed, expressed, and purified following *n*-dodecyl-β-D-maltoside (DDM) solubilization [26]. To test this construct for SMALP extraction, we first overproduced this protein heterologously in *Escherichia coli* (as described previously [26]), prepared *Vc*FeoB-containing membranes, and then tested the most commonly used SMA, SMA200, by altering its percentage in solution (*w/v*) with varied extraction temperatures (4 °C, room temperature (25 °C), and 37 °C) for formation of the styrene-maleic acid lipid particle (SMALP) particle under normalized conditions (*i.e.*, when comparing membranes produced from the same *E. coli* growth and at the same total membrane protein concentrations). As presented in Fig. 3, when SMA200 was used, there was a noticeable difference in the *Vc*FeoB-SMALP formation at different temperatures, with extraction worst at 4 °C, highly effective at 25 °C (room temperature), and best at 37 °C, as emphasized by the qualitative differences in intensities for the soluble and insoluble fractions as observed by SDS-PAGE (Fig. 3b). This result could be due to the phase transition of the lipid bilayer that behaves more like a solid-ordered gel at lower temperatures (*i.e.*, 4 °C) and is poorly SMA permeable, whereas the lipid bilayer behaves more like a liquid disordered at higher temperatures (*i.e.*, room temperature and 37 °C) and is significantly more SMA permeable. While extraction of *Vc*FeoB in SMA200 appeared to be qualitatively most effective at 37 °C, the protein was not stable for prolonged periods of time for downstream applications at this temperature (*vide infra*); thus, we chose to use room temperature (25 °C) for further extractions. Once encapsulated by the SMA200 SMALP, we then attempted to purify the membrane-embedded *Vc*FeoB-$(His)_6$ using immobilized metal affinity chromatography (IMAC). Despite exhaustive efforts in which multiple types of resins (NTA agarose, HisTrap FF, HisTrap HP) loaded with different metals (Ni^{2+} and Co^{2+}) in different forms (loose or pre-packed) were tested, we

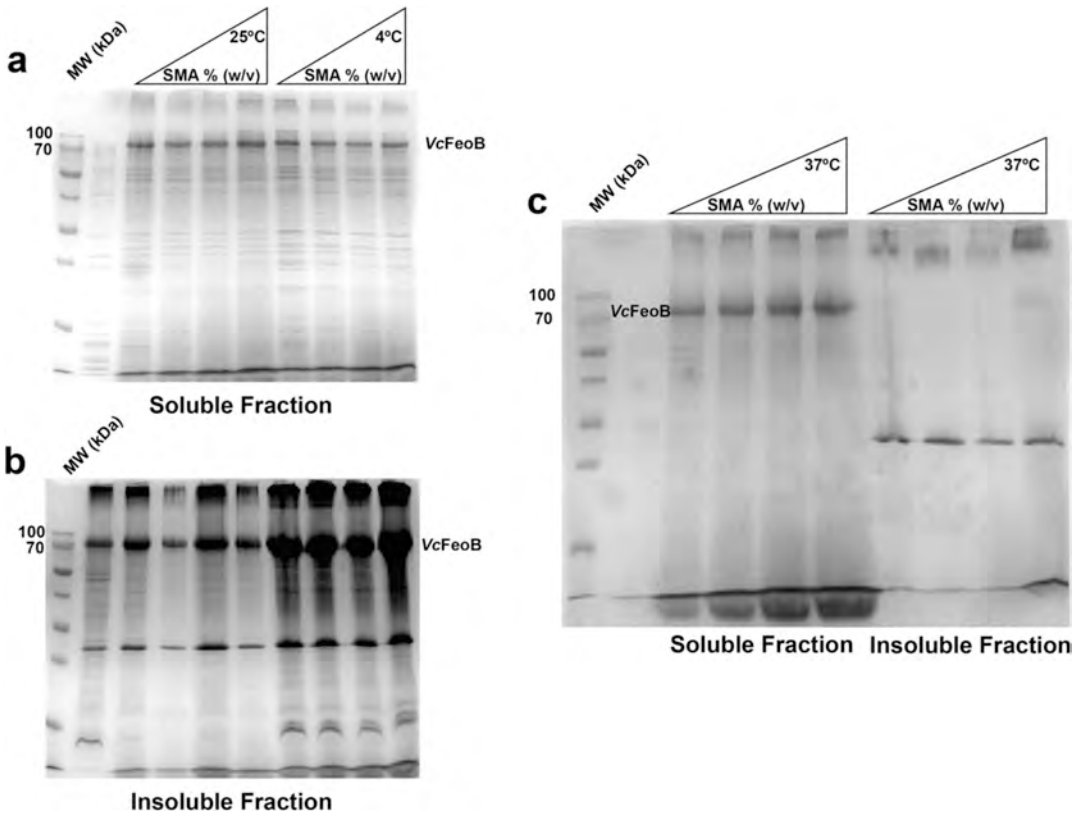

Fig. 3. SMA concentration- and temperature-dependent extraction tests of *Vc*FeoB(His)$_6$. a. Increasing SMA concentrations (1.0 % (*w/v*), 1.5 % (*w/v*), 2.0 % (*w/v*) and 2.5 % (*w/v*)) alongside temperatures (4 °C and 25 °C) were tested to achieve efficient solubilization. b. SDS-PAGE analysis of the insoluble fraction of a., indicates that 25 °C is more efficient than 4 °C for SMALP extraction of *Vc*FeoB across a range of SMA copolymer concentrations (1.0 % (*w/v*) to 2.5 % (*w/v*)). c. Temperature- and SMA-dependence trials of *Vc*FeoB-SMALP generation at 37 °C with both soluble and insoluble fractions labeled. Coomassie staining indicates that all concentrations of SMA200 are equally effective at extracting *Vc*FeoB at 37 °C. However, *Vc*FeoB was not stable for prolonged periods of time in SMA200 at 37 °C.

were never able to purify *Vc*FeoB-(His)$_6$ even though we observed robust extraction in SMA200. The most probable cause of this result is due to the intrinsic chelating nature of SMA-copolymers, as they have been shown to bind to a variety of metals [53]. Thus, the free-copolymer in solution may disrupt the (His)$_6$-tag binding to the resin by chelating the immobilized metal ion, leading to low yield. This drawback has been shown to be a recurring issue in other reports [54–56], which necessitated a different approach.

2.2. Redesign and expression testing of a SMALP-compatible VcFeoB construct

In an effort to circumvent our issues of poor IMAC-based purifications, we then sought to redesign the *Vc*FeoB expression plasmid to utilize a metal-free streptactin-based purification system. Multiple constructs were then synthesized based on the initial intact *Vc*FeoB gene (Fig. 4), and our derivatized forms were all subcloned into the pET-21a

Fig. 4. Schematic cartoons of the *Vc*FeoB constructs tested in this work. The core *Vc*FeoB-encoding gene is labeled in purple, the TEV protease sites are labeled in yellow, the (His)$_6$ tag site is labeled in blue, the Strep tag sites are labeled in orange, and the SUMO expression fusion site is labeled in green. In each schematic, 'N' and 'C' represent the N- and C-termini of each construct, respectively. (For interpretation of the references to colour in this figure legend, the reader is referred to the web version of this article.)

(+) vector in order to utilize the T7 promoter and isopropyl β-D-1-thiogalactopyranoside (IPTG)-based expression. The initial design was that of a (Strep)$_2$-tag that was placed at the N-terminus of the protein followed by a tobacco etch virus (TEV)-protease cleavage site, leaving the C-terminus unmodified (*i.e.*, (Strep)$_2$-TEV-*Vc*FeoB). Unfortunately, despite rigorous screening of expression cell lines, growth conditions, and expression temperatures Western blotting failed to detect any protein expression (data not shown). To assist in protein expression, we then added a small ubiquitin-like modifier (SUMO) tag in between the (Strep)$_2$-tag and *Vc*FeoB (*i.e.*, (Strep)$_2$-SUMO-*Vc*FeoB) However, again despite rigorous screening of expression cell lines, growth conditions, and expression temperatures, Western blotting failed to detect any protein expression (data not shown). We then reasoned that the presence of a tag on the N-terminus of *Vc*FeoB might destabilize the protein, so we designed a final construct in which the C-terminus of *Vc*FeoB was modified to include a TEV protease site followed by a (Strep)$_2$-tag (*i.e.*, *Vc*FeoB-TEV-(Strep)$_2$). Expression testing demonstrated that this strategy proved ultimately successful, and robust protein overproduction was found in the *E. coli* C43 (DE3) expression cell line (*vide infra*).

2.3. Overexpression and purification of VcFeoB in SMA200-copolymer lipid particles results in a detergent-free form of FeoB

Once expression testing demonstrated small-scale overproduction of *Vc*FeoB-TEV-(Strep)$_2$ in *E. coli* C43 (DE3) cells, large-scale expression, extraction of the protein in SMA200 SMALPs, and subsequent streptactin-based purification was accomplished (see general workflow in Fig. 5). Regarding large-scale cell growth and membrane preparation, this process followed a similar workflow as the small-scale trials (*vide supra*) with only slight modifications. Briefly, while the protein quantity

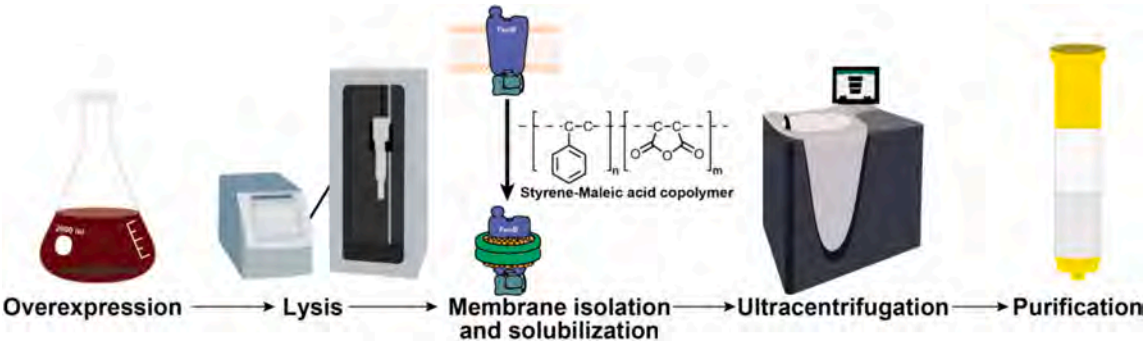

Fig. 5. General workflow for the purification of the *Vc*FeoB-TEV-(Strep)$_2$-SMALP complex. First, the protein is overproduced in *E. coli* C43 (DE3) expression cells grown in Terrific Broth (TB). Cells are then harvested and lysed using a sonicator. Membranes containing *Vc*FeoB-TEV-(Strep)$_2$ are then isolated through multiple rounds of centrifugation. *Vc*FeoB-TEV-(Strep)$_2$ encased in *E. coli* lipids is then extracted from membranes by addition of the SMA200 copolymer, after which the solution is then ultracentrifuged. The clarified solution containing the *Vc*FeoB-TEV-(Strep)$_2$-SMALP complex is then purified using a gravity column containing the Strep-tactin XT 4Flow high-capacity resin. The purified *Vc*FeoB-SMALP complex is then used for subsequent downstream applications.

per gram of cell pellet was comparable in both Luria broth (LB) and Terrific broth (TB) medias, we typically produced much larger cell pellets in TB due to its ability to sustain higher cell densities; therefore, all subsequent cell growths were done in TB media. The culture harvesting, cell lysing, and membrane preparations were the same as previously described [26]. Once the final membrane preparation was concluded, *E. coli* membranes containing *Vc*FeoB-TEV-(Strep)$_2$ were homogenized in buffer and diluted to 40–50 mg/mL concentration from crude membrane extracts prior to SMA200 additions. We then formed the SMA200-encapsulated SMALP complex by mixing 10 mL of the *Vc*FeoB-TEV-(Strep)$_2$-containing membrane solution with 2.5 % (*w/v*) SMA200 followed by centrifugation. Afterwards, we purified the *Vc*FeoB-TEV-(Strep)$_2$-SMALP complex by gravity using loose Strep-tactin XT 4Flow high-capacity resin, which we found to be more effective than fast protein liquid chromatography (FPLC)-based methods due to the ability to incubate the loose resin with the *Vc*FeoB-SMALP complex for more prolonged periods of time. The eluted protein was characterized by SDS-PAGE and subsequently verified by Western blotting (Fig. 6). In general, this procedure produced an average of 7.5 mg *Vc*FeoB-TEV-(Strep)$_2$ protein encapsulated by SMALP per L culture based on DC Lowry analyses.

2.4. SMALP encapsulation results in higher NTPase activity of VcFeoB

After successful purification of the detergent-free *Vc*FeoB-TEV-(Strep)$_2$-SMALP complex, we then sought to test whether FeoB would be active in an *E. coli* lipid bilayer. While many FeoB proteins are capable of hydrolyzing only GTP in a specific manner, *Vc*FeoB is more nucleotide promiscuous and hydrolyzes ATP as well as GTP based on previous studies of the *Vc*NFeoB domain [39], so we decided to test for both activities of the intact protein using a modified version of the malachite green assay [57]. To benchmark our results, we also compared this NTPase activity to DDM-solubilized protein to discern whether the presence of the lipid bilayer or that of the detergent micelle had any

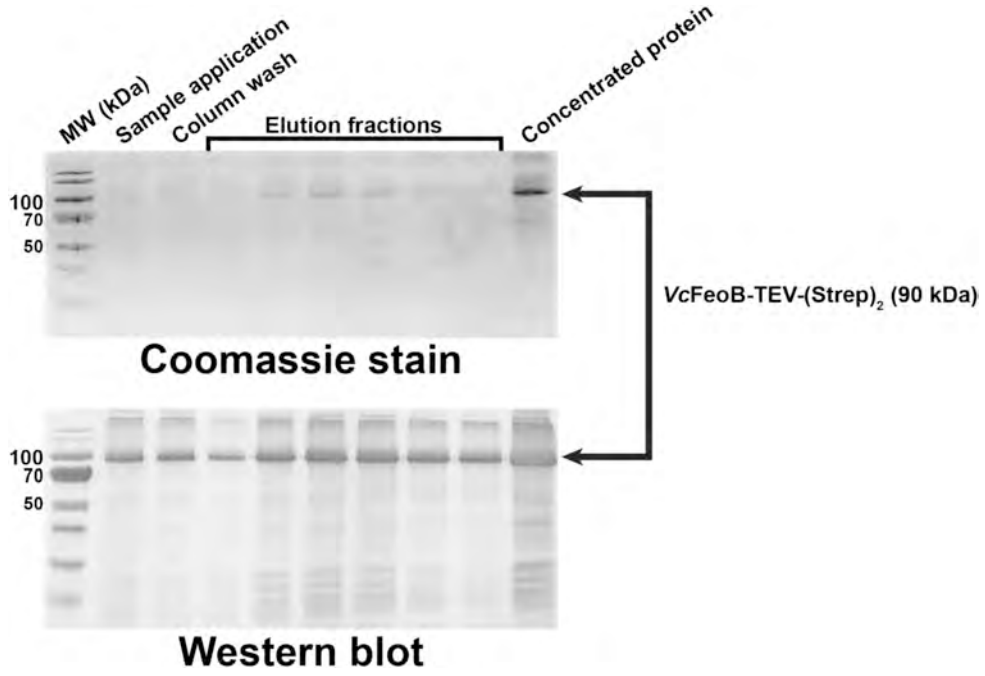

Fig. 6. SDS-PAGE (top) and Western blot analysis of the *Vc*FeoB-TEV-(Strep)$_2$-SMALP complex purification. The top panel displays a polyacrylamide gel of the Coomassie-stained purification of *Vc*FeoB-TEV-(Strep)$_2$-SMALP complex. The concentrated protein-SMALP complex is shown in the far-right lane, which represents the combined elution fractions shown in the top panel. The bottom panel shows the Western blot corresponding to the purification steps in the top SDS-PAGE analysis. The molecular weight of *Vc*FeoB-TEV-(Strep)$_2$ is *ca.* 90 kDa without the SMALP.

dramatic effect on nucleotide hydrolysis. In DDM, *Vc*FeoB-TEV-$(His)_6$ was active towards both GTP and ATP (Fig. 7a,c), and time-course assays revealed a k_{obs}^{GTP} value of 0.088 $s^{-1} \pm 0.003$ s^{-1} and a k_{obs}^{ATP} value of 0.108 $s^{-1} \pm 0.013$ s^{-1}, comparable to other detergent-solubilized, intact forms of FeoB (Table 1). Importantly, the detergent-free, SMALP-encapsulated *Vc*FeoB-TEV-$(Strep)_2$ purified protein was active and had generally higher activity towards GTP and ATP (Fig. 7b,d). Time-course assays of the SMALP protein complex revealed a k_{obs}^{GTP} value of 0.160 $s^{-1} \pm 0.023$ $s^{-1}$and a k_{obs}^{ATP} value of 0.130 $s^{-1} \pm 0.015$ s^{-1} (Table 1). Interestingly, the SMALP-solubilized *Vc*FeoB protein reached saturation in the presence of ATP by *ca.* 4 min, much sooner than in the presence of the DDM detergent micelle and unlike its behavior in the presence of GTP. Nonetheless, the k_{obs}^{ATP} is approximately three-fold higher when compared to the ATPase activity of the DDM-solubilized protein within the same timeframe. These results reveal that FeoB is generally more active towards nucleotide hydrolysis when intact and in a lipid bilayer, as we previously hypothesized [41], although there is not a dramatic difference in the observed nucleotide hydrolysis rates of the *Vc*FeoB-SMALP complex when compared to detergent-solubilized, purified intact FeoB (Table 1).

2.5. SMALP-encapsulated VcFeoB is more homogeneous and more monodisperse than DDM-purified VcFeoB

Finally, we sought to determine the homogeneity of the *Vc*FeoB-TEV-$(Strep)_2$-SMALP complex and to compare it to the DDM-solubilized *Vc*FeoB-$(His)_6$ form. We initially attempted to use analytical size-exclusion chromatography (SEC) to analyze both, but it was quickly apparent that the gel-filtration media stripped the *Vc*FeoB from the SMA copolymer, despite several attempts to prevent this outcome. Instead, we turned to the use of mass photometry to characterize the mass distributions of the *Vc*FeoB-TEV-$(Strep)_2$-SMALP complex and the DDM-solubilized *Vc*FeoB-$(His)_6$. As Fig. 8a demonstrates, the *Vc*FeoB-TEV-$(Strep)_2$-SMALP complex demonstrates one major peak centered at *ca.* 117 kDa (representing *ca.* 70 % of the total signal) with a second minor peak centered at *ca.* 170 kDa, based on calibrations using a β-amylase standard. The major peak observed is distinctly upshifted in mass compared to empty SMALP of *ca.* 65 kDa (*i.e.*, SMA200 filled with random *E. coli* lipids; Fig. 8a) and is most consistent with a single,

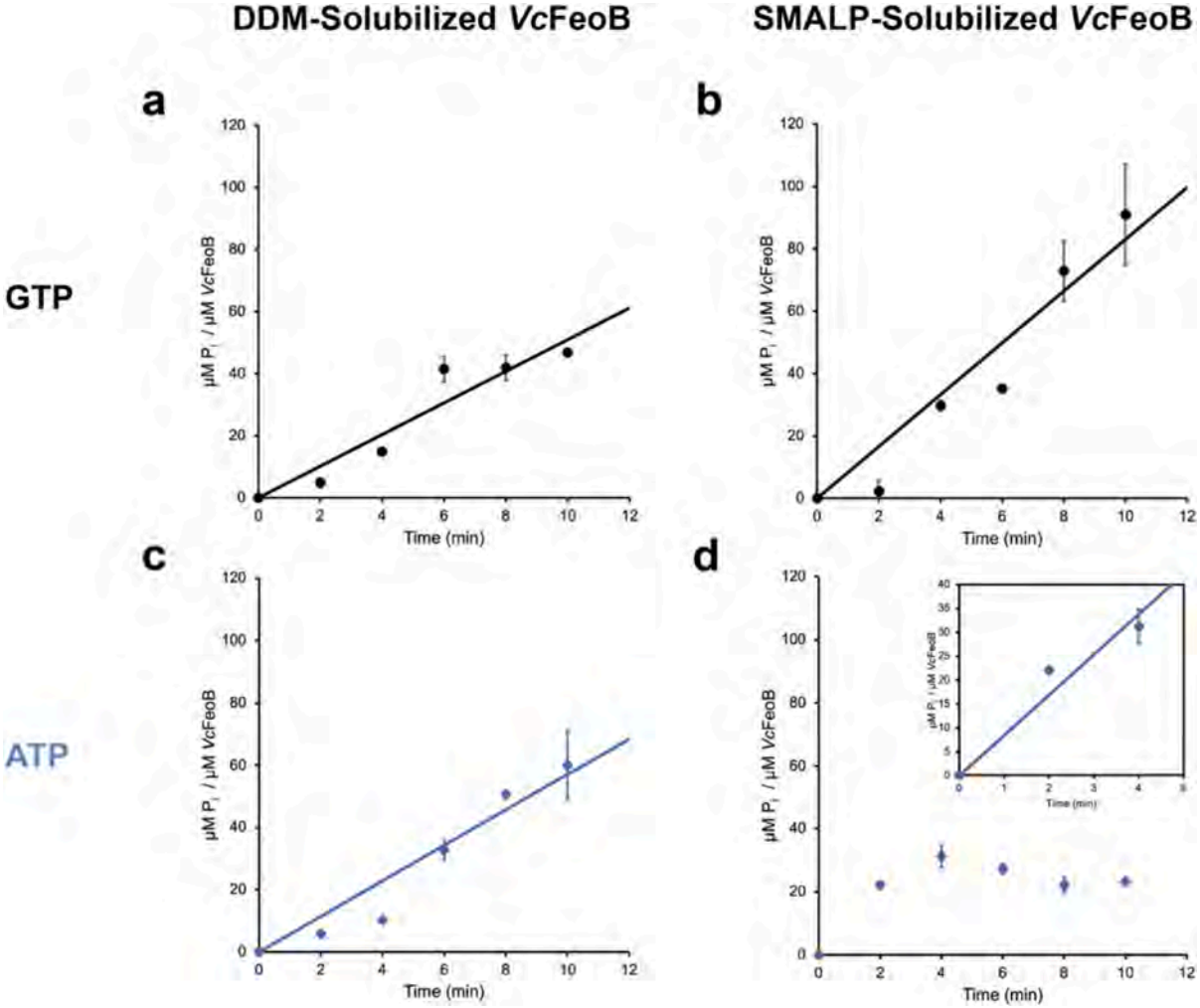

Fig. 7. Time-course assays of the NTPase activity of intact *Vc*FeoB. Initial rates were fitted to the linear region of the assay to compare observed catalytic rate constants between detergent-solubilized and SMALP-encapsulated *Vc*FeoB. Panels a and c show hydrolysis rates of DDM-solubilized *Vc*FeoB-TEV-$(His)_6$ in the presence of GTP (black circles; $k_{obs}^{GTP} = 0.088$ $s^{-1} \pm 0.003$ s^{-1}) and in the presence of ATP (blue diamonds; $k_{obs}^{ATP} = 0.108$ $s^{-1} \pm 0.013$ s^{-1}), respectively. Panels b and d show hydrolysis rates of SMALP-encapsulated *Vc*FeoB-TEV-$(Strep)_2$ in the presence of GTP (black circles; $k_{obs}^{GTP} = 0.160$ $s^{-1} \pm 0.023$ s^{-1}) and in the presence of ATP (blue diamonds; $k_{obs}^{ATP} = 0.130$ $s^{-1} \pm 0.015$ s^{-1}), respectively. The inset panel in d shows the linear regression of ATP hydrolysis from 0 to 4 min. Error bars represent ± one standard deviation of the mean of data taken in triplicate. (For interpretation of the references to colour in this figure legend, the reader is referred to the web version of this article.)

Table 1
Comparative table of FeoB/NFeoB k_{obs} values determined from various studies.

Organism	Protein	Solubilizing agent	k_{obs}^{GTP}	k_{obs}^{ATP}	Reference
Vibrio cholerae	FeoB	DDM	$0.088\ s^{-1} \pm 0.003\ s^{-1}$	$0.108\ s^{-1} \pm 0.013\ s^{-1}$	This study
Vibrio cholerae	FeoB	SMA200	$0.160\ s^{-1} \pm 0.023\ s^{-1}$	$0.130\ s^{-1} \pm 0.015\ s^{-1}$	This study
Vibrio cholerae	FeoABC fusion	DDM	$0.050\ s^{-1} \pm 0.0476\ s^{-1}$	$0.031\ s^{-1} \pm 0.0455\ s^{-1}$	Gómez-Garzón et al [58]
Pseudomonas aeruginosa	FeoB	DDM	[a] $0.0035\ s^{-1}$	–[b]	Seyedmohammad et al [40]
Escherichia coli	NFeoB	–[c]	$0.011\ s^{-1} \pm 0.001\ s^{-1}$	–[b]	Shin et al [59]
Streptococcus thermophilus	NFeoB	–[c]	$0.059\ s^{-1} \pm 0.110\ s^{-1}$	–[b]	Guilfoyle et al [60]
Klebsiella pneumoniae	FeoB	DDM	[a] $\approx 0.09\ s^{-1}$	–[b]	Smith et al [41]
Klebsiella pneumoniae	NFeoB	–[c]	[a] $1.7\ s^{-1} \times 10^{-5}$	–[b]	Hsueh et al [61]
Thermotoga maritima	NFeoB	–[c]	$0.017\ s^{-1} \pm 0.001\ s^{-1}$	–[b]	Hattori et al [62]

[a] No errors are reported for these values.
[b] The value was not determined.
[c] A solubilizing agent was not used.

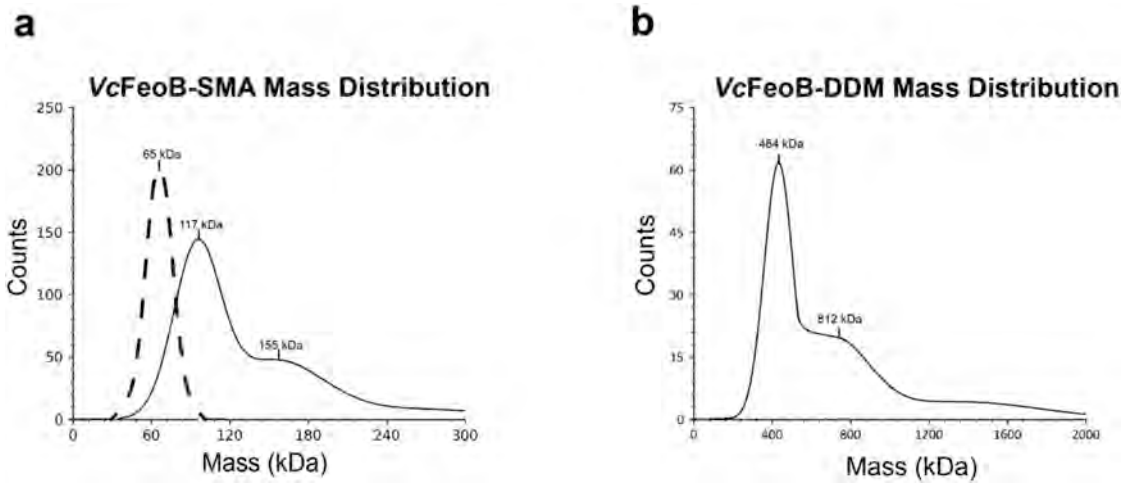

Fig. 8. Comparative oligomeric distributions of *Vc*FeoB in a SMALP and in a non-denaturing detergent. a. Mass profile of *Vc*FeoB in the SMALP complex determined by mass photometry. The first gaussian curve (dashed; 65 kDa) represents empty SMA lipid particles, while 117 kDa and 155 kDa indicate *Vc*FeoB-SMALP complex based on a known calibration curve. b. Mass profile of *Vc*FeoB solubilized by DDM determined by mass photometry. One gaussian curve is calculated with two peaks correlating to 484 kDa and 812 kDa based on the same calibration curve used in panel a.

monomeric encapsulated *Vc*FeoB-TEV-$(Strep)_2$, presuming that a significant fraction of lipid is likely displaced to afford room for FeoB during encapsulation. We are currently uncertain as to the identity of the broadly distributed peak centered at *ca.* 155 kDa, but this species is only a minority of the signal (< 20 %) and could represent a minor amount of oligomerized FeoB, or an unknown impurity. To utilize mass photometry in order to assess the oligomerization of DDM-solubilized *Vc*FeoB-$(His)_6$, we used a rapid drop-dilution method that revealed a much larger, heterogeneous mixture of *Vc*FeoB in a detergent micelle compared to a SMALP-encapsulated condition (Fig. 8b). Based on the same calibration standard used in Fig. 8a, there are two major species in solution at *ca.* 480 kDa and *ca.* 810 kDa, both of comparable populations (*ca.* 40 % and 50 %, respectively), with an even larger species (>1 MDa) comprising the remaining fraction of the DDM-solubilized protein in solution (Fig. 8b). A similar behavior is observed for the DDM-solubilized *Vc*FeoB-$(His)_6$ based on its SEC chromatogram (Figs. S1, S2). These results suggest that *Vc*FeoB may be unstable in DDM and aggregate under these conditions, and that a SMALP-based approach may be more favorable for biophysical characterization of *Vc*FeoB.

3. Discussion

The structure of intact FeoB, the main component of the Feo system, remains elusive. Only very recent reports have shown the FeoB can be produced recombinantly in large enough quantities necessary for traditional *in surfo* approaches applied commonly to X-ray crystallography of membrane proteins and, sometimes, to cryo-EM of membrane proteins [44,56]. However, determining the appropriate non-denaturing detergent to produce a homogeneous, monodisperse FeoB sample remains a tedious process requiring extensive trial-and-error [63]. Moreover, we have shown that nature of the solubilizing and purifying detergent can influence the nucleotide hydrolysis rates of intact FeoB [41], suggesting that the interaction between FeoB and the detergent micelle is not innocuous. These results are consistent with numerous other studies that have made it clear that the detergent micelle does not properly mimic the physiological environment of a membrane protein within a lipid bilayer, and that this mismatch may lead to protein instability and even attenuated activity [41,64,65]. Thus, approaches limiting the use of detergents should be considered when attempting to characterize membrane proteins biophysically.

In this work, we sought to purify the FeoB transporter from *V. cholerae* in a detergent-free manner by the direct extraction of this protein from an *E. coli* lipid bilayer using SMA copolymers. While we had initial success transferring a $(His)_6$-tagged version of *Vc*FeoB into a SMALP complex, the downstream affinity-based purification protocol proved incompatible with traditional IMAC approaches, which may be protein-dependent. Consistent with this notion, there are reports detailing both the successful [66–68] and unsuccessful [54–56] attempts at purifying His-tagged membrane proteins solubilized by SMA-copolymers. To circumvent this issue, we designed and synthesized multiple plasmid constructs and undertook extensive testing to optimize the expression of a C-terminally tagged version of *Vc*FeoB (*Vc*FeoB-TEV-$(Strep)_2$) that could be purified in a metal-free manner. It is possible that the C-terminal $(His)_6$-tag may be too short for FeoB in the SMALP to

access the Ni-NTA resin, and future studies could test with a longer His tag (*i.e.*, $(His)_8$ or $(His)_{10}$) might improve this protocol. Nevertheless, our dual C-terminal Strep-tagged approach proved successful.

Having achieved the first detergent-free purification of FeoB to our knowledge, we then sought to examine the NTPase activity of *Vc*FeoB in a lipid bilayer. Comparative activity analyses between the DDM-solubilized and SMA-encapsulated *Vc*FeoB were conducted, and we showed that the k_{obs}^{GTP} and k_{obs}^{ATP} values were modestly but consistently higher in a lipid bilayer than in DDM, a commonly-used detergent for membrane protein solubilization and structural determination. Finally, we tested whether SMA-encapsulated or DDM-solubilized *Vc*FeoB displayed greater solution monodispersity, an important physical characteristic when preparing biological molecules for structural studies. We found that SMA-encapsulated *Vc*FeoB displayed a mostly monomeric form based on mass photometry analysis whereas DDM-solubilized *Vc*FeoB displayed large amounts of aggregation and high amounts of heterogeneity based on both mass photometry and size-exclusion chromatography, illustrating a stark contrast between the two sample preparation approaches. Thus, this study represents the first to compare and to contrast the behavior of FeoB in a lipid bilayer and in a detergent micelle.

The results presented in this report give additional insight into *Vc*FeoB function and provide a promising experimental approach that could be leveraged for future structural and biophysical studies of FeoB more generally. First, while the N-terminal domain of *Vc*FeoB (*i.e., Vc*NFeoB) has been shown to be NTP promiscuous and to hydrolyze GTP and ATP [39], whether the intact, independent *Vc*FeoB behaves similarly in a lipid bilayer was not previously known, but this functional continuity is now confirmed. Second, while we have long speculated that the presence of the lipid bilayer could influence nucleotide hydrolysis activity (and even the ability of FeoB to translocate Fe^{2+}) [41], we now know that the presence of an intact membrane indeed has at least a modest effect on the ability of *Vc*FeoB to hydrolyze GTP and ATP. Finally, data presented here suggest that *Vc*FeoB is mostly monomeric in a lipid bilayer, at least when recombinantly overproduced on its own in *E. coli*. The oligomeric state of FeoB remains controversial and has been suggested to function as a trimer (based on homology modeling and native-PAGE) [69,70] and as a monomer (based on *in vitro* work and native-PAGE) [41,63]. However, it is possible that differences in the lipid compositions between *V. cholerae* (the native organism) and *E. coli* (the recombinant organism) may influence oligomerization. Alternatively, other components of the Feo system (such as FeoA and/or FeoC) may be necessary to initiate oligomerization, as previously suggested [70]. While *E. coli* does encode for and natively produces these proteins, FeoA and FeoC may not be present *in vivo* in sufficient quantities to be able to facilitate *Vc*FeoB oligomerization during overproduction in the recombinant host. Regardless, the results presented in this work demonstrate the ability to produce high-quality *Vc*FeoB active towards nucleotide hydrolysis when encapsulated in a lipid bilayer, and this approach could be leveraged for future structural studies, such as X-ray crystallography (less common) or cryo-EM (more common), which would represent a major advancement in the Feo field once realized.

4. Materials and methods

4.1. Materials

All constructs of FeoB from *Vibrio cholerae serotype O1* (strain M66–2) (Uniprot ID C3LP27) were commercially synthesized by GenScript. Ampicillin, isopropyl β-D-*l*-thiogalactopyranoside (IPTG), phenylmethylsulfonyl fluoride (PMSF), biotin and *n*-dodecyl-β-D-maltopyranoside (DDM) were purchased from RPI. Styrene:maleic acid (SMA) copolymers at a 2:1 ratio (SMA200) and 3:1 ratio (SMA300) were purchased from CubeBiotech. The Strep-TactinXT 4Flow high-capacity resin was purchased from IBA Lifesciences GmbH. Other materials for cell growth and membrane isolation were purchased from Cytiva, Fisher Scientific, MilliporeSigma, and/or VWR. Unless otherwise specified, materials were used as received without further modifications.

4.2. Cloning and expression of VcFeoB with various N- and C-terminal affinity tags

The initial gene corresponding to WT *Vc*FeoB (Uniprot ID C3LP27) was synthesized by GenScript and further modified as warranted. Initially, the gene was further engineered first to include a tobacco etch virus (TEV)-protease cleavage site (ENLYFQS) at the C-terminal end of the gene product and then subcloned into the pET-21a(+) vector such that a C-terminal $(His)_6$ tag was produced when the entire gene product was translated in-frame (*i.e.*, *Vc*FeoB-$(His)_6$) to allow for tag removal, if necessary. To avoid the chelating effects of the SMA copolymers to metal-based resins, the initial synthetic gene was then modified to include several permutations of the twin-Strep-tag system. First, the WT *Vc*FeoB gene was engineered to include an N-terminal twin Strep-tag (N-WSHPQFEKGGGSGGGSGGSAWSHPQFEK-C) followed by a TEV-protease cleavage site, which was then subcloned into the pET-21a(+) vector such that all three regions of the polypeptide would be translated when read in-frame (*i.e.*, $(Strep)_2$-TEV-*Vc*FeoB). Next, the initial WT *Vc*FeoB gene was engineered to include an N-terminal twin Strep-tag followed by a small ubiquitin-like modifier (SUMO)-tag (Uniprot ID Q12306) that was inserted after the twin-Strep-tag to facilitate expression, which was then subcloned into the pET-21a(+) vector such that all three regions of the polypeptide would be translated when read in-frame (*i.e.*, $(Strep)_2$-SUMO-*Vc*FeoB). Finally, the initial WT *Vc*FeoB gene was engineered to include a C-terminal TEV-protease cleavage site followed by a twin Strep-tag, which was then subcloned into the pET-21a(+) vector such that all three regions of the polypeptide would be translated when read in-frame (*i.e.*, *Vc*FeoB-TEV-$(Strep)_2$). In all cases, subcloning of the engineered DNA inserts into the pET-21a(+) vector was achieved by using the *Nde*I and *Xho*I restriction sites.

All plasmid constructs were transformed *via* electroporation into multiple *Escherichia coli* expression cell-lines (BL21(DE3), C41(DE3), and C43(DE3)) prior to expression testing. Electroporated cells were then plated onto Luria-Bertani (LB) agar plates with supplemented 100 μg/mL ampicillin (final) and incubated overnight at 37 °C. The next day, colonies from each plate were picked and used to inoculate precultures of 5 mL LB and/or terrific broth (TB) media supplemented with 100 μg/mL ampicillin (final) for expression testing. Precultures were grown overnight at 37 °C with shaking of 200 RPM for *ca.* 16–20 h. The next day, 250 mL flasks containing 100 mL LB supplemented with 100 μg/mL ampicillin (final) were inoculated with *ca.* 2 mL of the overnight preculture. Flasks were then grown at 37 °C with shaking of 200 RPM; once the optical density at 600 nm (OD_{600}) reached ≈ 0.4–0.8, protein production was initiated by the addition of isopropyl β-D-1-thiogalactopyranoside (IPTG) to a final concentration of 1 mM. Protein production then occurred with cells growing at 37 °C with 200 RPM shaking. After 3 h, cells were harvested into 50 mL falcon tubes by centrifugation at 4800 ×*g* for 10 min at 4 °C, flash frozen, and stored at −20 °C. To test for protein overproduction, frozen cells were then thawed and resuspended to a final volume of 10 mL with resuspension buffer (50 mM Tris pH = 8.0, 100 mM sucrose). Prior to cell lysis, phenylmethylsulfonyl fluoride (PMSF) was added to the resuspended cells to a final concentration of 1 mM. Cells were lysed at 4 °C with a Q700 ultrasonic cell disruptor (QSonica) equipped with the microtip operating at 40 % maximal amplitude, 30 s pulse on, 30 s pulse off for 2 min with cells immersed in an ice water bath to prevent overheating. Lysed cells were then transferred to a microcentrifuge tube and partially clarified by spinning at 4000 ×*g* for 40 min. The supernatant containing both soluble and membrane fractions was then transferred to another microcentrifuge tube and centrifuged at 15000 ×*g* for 2 h. The supernatant was then discarded and the membrane-containing fraction was mixed with 100 μL of 10 % (*w/v*) sodium dodecyl sulfate (SDS) and vortexed until homogenous. Membrane-bound proteins were then

analyzed by 15 % sodium dodecyl sulfate polyacrylamide gel electrophoresis (SDS-PAGE) and verified *via* Western blot analysis, as previously described [63], using either the anti-poly-histidine-peroxidase antibody (Millipore Sigma) or the anti-Streptactin-peroxidase antibody (VWR).

Constructs that tested positive for *Vc*FeoB overproduction (*Vc*FeoB-$(His)_6$ and *Vc*FeoB-TEV-$(Strep)_2$) were then scaled up for large-scale protein production. Briefly, 2 L of TB media supplemented with 100 μg/mL (final) ampicillin were inoculated with 25 mL of preculture as described (*vide supra*). Cells were allowed to grow until reaching an $OD_{600} \approx 0.4–0.8$, after which cells were then cold-shocked at 4 °C for 2 h. Next, IPTG was added to 1 mM (final) concentration to induce protein production, and cells were allowed to shake at 18 °C at 200 RPM for *ca.* 20 h. The following day, cells were pelleted by centrifugation at 5000 ×*g* for 12 min and then resuspended with 50 mL of Tris-based resuspension buffer (*vide supra*) for the *Vc*FeoB-$(His)_6$ construct and HEPES-based resuspension buffer (50 mM HEPES pH = 8.0, 100 mM sucrose) for the *Vc*FeoB-TEV-$(Strep)_2$ construct. Prior to lysis, cells were diluted to 100 mL in a stainless-steel beaker, PMSF was added to 1 mM (final), and resuspended cells were sonicated at 4 °C using an Q700 ultrasonic cell disruptor operating at a maximal amplitude of 80 %, 30 s pulse on and 30 s pulse off for 12 min while immersed in an ice water bath. Cellular debris was then separated from cellular membranes by centrifugation at 10000 ×*g* for 1 h at 4 °C. The supernatant was then transferred to a series of ultracentrifuge tubes and cellular membranes were pelleted by ultracentrifugation at 163000 ×*g* for 1 h at 4 °C. The supernatant was then discarded and the membrane pellet containing the protein of interest was homogenized and diluted in resuspension buffer to a crude membrane concentration of 40–50 mg/mL prior to being flash-frozen in $N_{2(l)}$ and stored at −80 °C. All protein concentrations were determined using the detergent-compatible Lowry assay (DC Lowry assay, Bio-Rad).

4.3. Purification of detergent-solubilized *Vc*FeoB-$(His)_6$

All steps in the purification of *Vc*FeoB-$(His)_6$ were conducted at 4 °C unless otherwise stated. Frozen bacterial membranes containing a *Vc*FeoB-$(His)_6$ were thawed and initially diluted to 100 mL (final) with resuspension buffer containing an additional 300 mM NaCl (final). To that solution, a stock of 10 % (*w/v*) *n*-dodecyl-β-D-maltoside (DDM) was added dropwise until the final concentration of DDM was 1 % (*w/v*). The membrane suspension was solubilized while stirring vigorously at room temperature for 2 h. Solubilized *Vc*FeoB-$(His)_6$ was then separated from insoluble material by ultracentrifugation at 163000 ×*g* for 1 h at 4 °C. DDM-solubilized *Vc*FeoB-$(His)_6$ was then applied to a preequilibrated 5 mL immobilized metal affinity chromatography (IMAC) HisTrap column (Cytiva) pre-equilibrated with 5 column volumes (CV) of IMAC wash buffer (50 mM Tris pH = 8.0, 300 mM NaCl, 100 mM sucrose, and 0.1 % (*w/v*) DDM). After washing of the column extensively, *Vc*FeoB-$(His)_6$ was eluted from the column with IMAC elution buffer (50 mM Tris pH = 8.0, 300 mM NaCl, 100 mM sucrose, 150 mM imidazole, and 0.1 % (*w/v*) DDM). Fractions containing *Vc*FeoB-$(His)_6$ were then pooled and subsequently buffer exchanged into IMAC wash buffer to remove excess imidazole by using a 100 kDa molecular weight cutoff (MWCO) spin concentrator *via* repeated concentration and dilution. The IMAC purified *Vc*FeoB-$(His)_6$ was concentrated to 5 mg/mL prior to being flash-frozen in $N_{2(l)}$ and stored at −80 °C. Frozen *Vc*FeoB was thawed in ice and applied to a Superose 6 analytical column pre-equilibrated with SEC buffer (25 mM Tris pH = 7.5, 100 mM NaCl, 5 % glycerol, 0.01 % (*w/v*) DDM and 1 mM TCEP). Chromatogram peak samples were collected and analyzed *via* SDS-PAGE.

4.4. SMA extraction testing

Various concentrations of SMA200 and SMA300 were tested at variable temperatures to optimize the extraction of *Vc*FeoB into the SMALP. Membranes containing *Vc*FeoB were prepared as stated (*vide supra*). Membranes were then aliquoted prior to the addition of SMA200 or SMA300 at various concentrations (1.0 % (*w/v*), 1.5 % (*w/v*), 2.0 % (*w/v*), 2.5 % (*w/v*)) and at various temperatures (4 °C, 25 °C, and 37 °C). SMA extraction was allowed to occur overnight with gentle rocking. The next day, the solution was centrifuged in a microcentrifuge at 14000 ×*g* for 90 min, 4 °C. The solubilized fraction was separated from the insoluble fraction *via* decanting, and both were analyzed with SDS-PAGE after normalization.

4.5. Purification of SMALP-encapsulated *Vc*FeoB-TEV-$(Strep)_2$

10 mL of frozen bacterial membranes containing *Vc*FeoB-TEV-$(Strep)_2$ were initially thawed, to which a stock solution of SMALP200 was added dropwise until reaching a final SMALP200 concentration of 2.5 % (w/v). The solution containing SMALP200 and *Vc*FeoB-TEV-$(Strep)_2$ was incubated at room temperature with gentle stirring for 2 h, after which the solution was then diluted to 25 mL with HEPES resuspension buffer and clarified *via* ultracentrifugation at 163000 ×*g* for 1 h at 4 °C. The supernatant containing the SMALP200-encapsulated *Vc*FeoB-TEV-$(Strep)_2$ was then applied to 4 mL of Strep-TactinXT 4Flow high-capacity resin and incubated overnight at 4 °C with gentle rocking. The resin and the solution were then applied to an Econo-Column (Bio-Rad) and allowed to rest for 1 h before the supernatant was collected. The column was then washed with 5 CV of Strep wash buffer (25 mM HEPES pH = 8.0, 100 mM NaCl, and 100 mM sucrose). 3 CV of Strep elution buffer (25 mM HEPES pH = 8.0, 100 mM NaCl, 100 mM sucrose, and 50 mM biotin) was then added to the resin, the column was stoppered, and the resin and solution were mixed gently. The resin and the solution were then allowed to rest for 1 h prior to fractionation of the eluted solution in 6 × 1 mL fractions. Fractions containing *Vc*FeoB-TEV-$(Strep)_2$ were then pooled and concentrated with a 100 kDa MWCO spin concentrator, typically to 1–3 mg/mL concentrations. The resin was regenerated by washing extensively with 15 CV of 3 M $MgCl_2$. *Vc*FeoB-TEV-$(Strep)_2$ was then buffer exchanged into Strep wash buffer by using a 100 kDa MWCO spin concentrator *via* repeated concentration and dilution. The final purified *Vc*FeoB-TEV-$(Strep)_2$ was concentrated to 5 mg/mL prior to flash-freezing in $N_{2(l)}$ and at −80 °C until further use.

4.6. NTPase activity assays

GTPase and ATPase activities were detected using a modified form of the malachite green assay [71] as described previously [41]. Briefly, both *Vc*FeoB-$(His)_6$ and *Vc*FeoB-TEV-$(Strep)_2$ were assayed in triplicate using a fixed concentration of GTP or ATP over a time range of 0–10 min. DDM-solubilized and purified *Vc*FeoB-$(His)_6$ was assayed after preincubation of added soybean azolectin to 0.1 mg/mL (final) and DDM to 0.01 % (*w/v*, final). SMALP-encapsulated and purified *Vc*FeoB-TEV-$(Strep)_2$ was not assayed with preincubation of any lipid nor detergent due to being encapsulated in the native *E. coli* lipid bilayer and due the need to preserve the integrity of the SMALP complex that dissociates in the presence of detergents. Once the assay solutions were developed, the concentration of inorganic phosphate [P_i] was determined by the absorption of the malachite-green-inorganic-phosphate-molybdate complex at 660 nm by using a Cary 60 UV–Vis spectrophotometer (Agilent) and interpolating from a standard curve.

4.7. Mass photometry of *Vc*FeoB

The distribution of particle size in the purified samples of *Vc*FeoB was determined *via* mass photometry by use of a Refeyn TwoMP instrument. First, a linear calibration curve ($R^2 = 0.999$) was created using β-amylase as a standard for three points: 58 kDa (monomer), 117 kDa (dimer), and 175 (trimer). Purified SMALP-encapsulated *Vc*FeoB-TEV-$(Strep)_2$ was then deposited onto a glass slide at a concentration of *ca.* 100 nM, and binding and unbinding events were recorded with the

AcquireMP software for 60 s in triplicate. Purified *Vc*FeoB(His)$_6$ in DDM was diluted first to 100 nM, and then 1:10 and 1:100 dilutions were made in SEC buffer lacking DDM. Recordings were analyzed using the Discover MP software, and the molecular weights of the *Vc*FeoB-TEV-(Strep)$_2$ SMALP-encapsulated protein and the *Vc*FeoB(His)$_6$ protein were interpolated using the linear β-amylase standard curve.

CRediT authorship contribution statement

Mark Lee: Writing – review & editing, Writing – original draft, Visualization, Validation, Investigation, Formal analysis. **Candice M. Armstrong:** Visualization, Validation, Investigation, Formal analysis. **Aaron T. Smith:** Writing – review & editing, Visualization, Supervision, Project administration, Funding acquisition.

Declaration of competing interest

The authors declare that they have no known competing financial interests or personal relationships that could have appeared to influence the work reported in this paper.

Acknowledgements

This work was primarily supported by NSF CAREER grant CHE1844624 (A. T. S.), and in part by NIH-NIGMS grant R35 GM133497 (A. T. S) and NIH-NIGMS grant T32 GM066706 (A. T. S., M. L., and C. M. A.). Sequence searches utilized both database and analysis functions of the Universal Protein Resource (UniProt) Knowledgebase and Reference Clusters (http://www.uniprot.org) and the National Center for Biotechnology Information (http://www.ncbi.nlm.nih.gov/).

Appendix A. Supplementary data

Supplementary data to this article can be found online at https://doi.org/10.1016/j.bbamem.2024.184404.

Data availability

Data will be made available on request.

References

[1] J.R. Sheldon, H.A. Laakso, D.E. Heinrichs, Iron acquisition strategies of bacterial pathogens, Microbiol. Spectr. 4 (2) (2016), https://doi.org/10.1128/microbiolspec.VMBF-0010-2015.
[2] S.M. Zughaier, P. Cornelis, Editorial: role of Iron in bacterial pathogenesis, Front. Cell. Infect. Microbiol. 8 (2018) 344, https://doi.org/10.3389/fcimb.2018.00344.
[3] C. Ratledge, L.G. Dover, Iron metabolism in pathogenic bacteria, Ann. Rev. Microbiol. 54 (2000) 881–941, https://doi.org/10.1146/annurev.micro.54.1.881.
[4] S. Booker, J. Broderick, J. Stubbe, Ribonucleotide reductases: radical enzymes with suicidal tendencies, Biochem. Soc. Trans. 21 (Pt 3) (3) (1993) 727–730, https://doi.org/10.1042/bst0210727.
[5] F. Berkovitch, Y. Nicolet, J.T. Wan, J.T. Jarrett, C.L. Drennan, Crystal structure of biotin synthase, an S-adenosylmethionine-dependent radical enzyme, Science 303 (5654) (2004) 76–79, https://doi.org/10.1126/science.1088493.
[6] O. Einsle, D.C. Rees, Structural enzymology of Nitrogenase enzymes, Chem. Rev. 120 (12) (2020) 4969–5004, https://doi.org/10.1021/acs.chemrev.0c00067.
[7] S.C. Andrews, A.K. Robinson, F. Rodríguez-Quiñones, Bacterial iron homeostasis, FEMS Microbiol. Rev. 27 (2–3) (2003) 215–237.
[8] I.J. Schalk, G.L.A. Mislin, Bacterial Iron uptake pathways: gates for the import of bactericide compounds, J. Med. Chem. 60 (11) (2017) 4573–4576, https://doi.org/10.1021/acs.jmedchem.7b00554.
[9] M.A. Fischbach, H. Lin, D.R. Liu, C.T. Walsh, How pathogenic bacteria evade mammalian sabotage in the battle for iron, Nat. Chem. Biol. 2 (3) (2006) 132–138, https://doi.org/10.1038/nchembio771.
[10] K.D. Krewulak, H.J. Vogel, Structural biology of bacterial iron uptake, Biochim. Biophys. Acta 1778 (9) (2008) 1781–1804, https://doi.org/10.1016/j.bbamem.2007.07.026.
[11] S. Létoffé, G. Heuck, P. Delepelaire, N. Lange, C. Wandersman, Bacteria capture iron from heme by keeping tetrapyrrol skeleton intact, Proc. Natl. Acad. Sci. USA 106 (28) (2009) 11719–11724, https://doi.org/10.1073/pnas.0903842106.
[12] S. Cescau, H. Cwerman, S. Létoffé, P. Delepelaire, C. Wandersman, F. Biville, Heme acquisition by hemophores, Biometals 20 (3–4) (2007) 603–613, https://doi.org/10.1007/s10534-006-9050-y.
[13] A.D. Smith, A. Wilks, Differential contributions of the outer membrane receptors PhuR and HasR to heme acquisition in Pseudomonas aeruginosa, J. Biol. Chem. 290 (12) (2015) 7756–7766, https://doi.org/10.1074/jbc.M114.633495.
[14] K.L. Richard, B.R. Kelley, J.G. Johnson, Heme uptake and utilization by gram-negative bacterial pathogens, Front. Cell. Infect. Microbiol. 9 (2019) 81, https://doi.org/10.3389/fcimb.2019.00081.
[15] I. Schröder, E. Johnson, S. de Vries, Microbial ferric iron reductases, FEMS Microbiol. Rev. 27 (2–3) (2003) 427–447, https://doi.org/10.1016/S0168-6445(03)00043-3.
[16] T.J. Cain, A.T. Smith, Ferric iron reductases and their contribution to unicellular ferrous iron uptake, J. Inorg. Biochem. 218 (2021) 111407, https://doi.org/10.1016/j.jinorgbio.2021.111407.
[17] J.J. Bullen, P.B. Spalding, C.G. Ward, H.J. Rogers, The role of eh, pH and iron in the bactericidal power of human plasma, FEMS Microbiol. Lett. 73 (1–2) (1992) 47–52, https://doi.org/10.1016/0378-1097(92)90581-8.
[18] C.K. Lau, K.D. Krewulak, H.J. Vogel, Bacterial ferrous iron transport: the Feo system, FEMS Microbiol. Rev. 40 (2) (2016) 273–298, https://doi.org/10.1093/femsre/fuv049.
[19] A.E. Sestok, M.A. Lee, A.T. Smith, Prokaryotic ferrous iron uptake: exploiting pools of reduced iron across multiple microbial environments. In *Advances in Environmental Microbiology: Microbial Metabolism of Metals and Metalloids*, Hurst, C. J. Ed, 2020.
[20] A.E. Sestok, R.O. Linkous, A.T. Smith, Toward a mechanistic understanding of Feo-mediated ferrous iron uptake, Metallomics 10 (7) (2018) 887–898, https://doi.org/10.1039/c8mt00097b.
[21] J.B. Brown, M.A. Lee, A.T. Smith, Ins and outs: recent advancements in membrane protein-mediated prokaryotic ferrous Iron transport, Biochemistry 60 (44) (2021) 3277–3291, https://doi.org/10.1021/acs.biochem.1c00586.
[22] H. Kim, H. Lee, D. Shin, The FeoA protein is necessary for the FeoB transporter to import ferrous iron, Biochem. Biophys. Res. Commun. 423 (4) (2012) 733–738, https://doi.org/10.1016/j.bbrc.2012.06.027.
[23] A.E. Sestok, J.B. Brown, J.O. Obi, S.M. O'Sullivan, E.D. Garcin, D.J. Deredge, A. T. Smith, A fusion of the Bacteroides fragilis ferrous iron import proteins reveals a role for FeoA in stabilizing GTP-bound FeoB, J. Biol. Chem. 298 (4) (2022) 101808, https://doi.org/10.1016/j.jbc.2022.101808.
[24] K.W. Hung, J.Y. Tsai, T.H. Juan, Y.L. Hsu, C.D. Hsiao, T.H. Huang, Crystal structure of the *Klebsiella pneumoniae* NFeoB/FeoC complex and roles of FeoC in regulation of Fe^{2+} transport by the bacterial Feo system, J. Bacteriol. 194 (23) (2012) 6518–6526, https://doi.org/10.1128/JB.01228-12.
[25] E.A. Weaver, E.E. Wyckoff, A.R. Mey, R. Morrison, S.M. Payne, FeoA and FeoC are essential components of the *Vibrio cholerae* ferrous iron uptake system, and FeoC interacts with FeoB, J. Bacteriol. 195 (21) (2013) 4826–4835, https://doi.org/10.1128/jb.00738-13.
[26] Brown, J. B.; Lee, M. A.; Smith, A. T. The structure of Vibrio cholerae FeoC reveals conservation of the helix-turn-helix motif but not the cluster-binding domain. J. Biol. Inorg. Chem. 2022, 27 (4–5), 485–495. DOI:https://doi.org/10.1007/s00775-022-01945-4.
[27] A.T. Smith, R.O. Linkous, N.J. Max, A.E. Sestok, V.A. Szalai, K.N. Chacón, The FeoC [4Fe-4S] cluster is redox-active and rapidly oxygen-sensitive, Biochemistry 58 (49) (2019) 4935–4949, https://doi.org/10.1021/acs.biochem.9b00745.
[28] B. Stevenson, E.E. Wyckoff, S.M. Payne, Vibrio cholerae FeoA, FeoB, and FeoC interact to form a complex, J. Bacteriol. 198 (7) (2016) 1160–1170, https://doi.org/10.1128/JB.00930-15.
[29] S. Seyedmohammad, N.A. Fuentealba, R.A. Marriott, T.A. Goetze, J.M. Edwardson, N.P. Barrera, H. Venter, Structural model of FeoB, the iron transporter from Pseudomonas aeruginosa, predicts a cysteine lined, GTP-gated pore, Biosci. Rep. 36 (2) (2016), https://doi.org/10.1042/BSR20160046.
[30] M.R. Ash, A. Guilfoyle, R.J. Clarke, J.M. Guss, M.J. Maher, M. Jormakka, Potassium-activated GTPase reaction in the G protein-coupled ferrous iron transporter B, J. Biol. Chem. 285 (19) (2010) 14594–14602, https://doi.org/10.1074/jbc.M110.111914.
[31] M.R. Ash, M.J. Maher, J.M. Guss, M. Jormakka, A suite of switch I and switch II mutant structures from the G-protein domain of FeoB, Acta Crystallogr. D Biol. Crystallogr. 67 (Pt 11) (2011) 973–980, https://doi.org/10.1107/s0907444911039461.
[32] M.R. Ash, M.J. Maher, J.M. Guss, M. Jormakka, The initiation of GTP hydrolysis by the G-domain of FeoB: insights from a transition-state complex structure, PLoS One 6 (8) (2011) e23355, https://doi.org/10.1371/journal.pone.0023355.
[33] M.R. Ash, M.J. Maher, J.M. Guss, M. Jormakka, The structure of an N11A mutant of the G-protein domain of FeoB, Acta Crystallogr. Sect. F Struct. Biol. Cryst. Commun. 67 (Pt 12) (2011) 1511–1515, https://doi.org/10.1107/s1744309111042965.
[34] C.N. Deshpande, A.P. McGrath, J. Font, A.P. Guilfoyle, M.J. Maher, M. Jormakka, Structure of an atypical FeoB G-domain reveals a putative domain-swapped dimer, Acta Crystallogr. Sect. F Struct. Biol. Cryst. Commun. 69 (Pt 4) (2013) 399–404, https://doi.org/10.1107/S1744309113005939.
[35] E.T. Eng, A.R. Jalilian, K.A. Spasov, V.M. Unger, Characterization of a novel prokaryotic GDP dissociation inhibitor domain from the G protein coupled membrane protein FeoB, J. Mol. Biol. 375 (4) (2008) 1086–1097, https://doi.org/10.1016/j.jmb.2007.11.027.
[36] K.W. Hung, Y.W. Chang, E.T. Eng, J.H. Chen, Y.C. Chen, Y.J. Sun, C.D. Hsiao, G. Dong, K.A. Spasov, V.M. Unger, et al., Structural fold, conservation and Fe(II)

binding of the intracellular domain of prokaryote FeoB, J. Struct. Biol. 170 (3) (2010) 501–512, https://doi.org/10.1016/j.jsb.2010.01.017.
[37] T.C. Marlovits, W. Haase, C. Herrmann, S.G. Aller, V.M. Unger, The membrane protein FeoB contains an intramolecular G protein essential for Fe(II) uptake in bacteria, Proc. Natl. Acad. Sci. USA 99 (25) (2002) 16243–16248, https://doi.org/10.1073/pnas.242338299.
[38] N. Petermann, G. Hansen, C.L. Schmidt, R. Hilgenfeld, Structure of the GTPase and GDI domains of FeoB, the ferrous iron transporter of *legionella pneumophila*, FEBS Lett. 584 (4) (2010) 733–738, https://doi.org/10.1016/j.febslet.2009.12.045.
[39] M. Lee, K. Magante, C. Gómez-Garzón, S.M. Payne, A.T. Smith, Structural determinants of Vibrio cholerae FeoB nucleotide promiscuity, J. Biol. Chem. (2024) 107663, https://doi.org/10.1016/j.jbc.2024.107663.
[40] S. Seyedmohammad, D. Born, H. Venter, Expression, purification and functional reconstitution of FeoB, the ferrous iron transporter from *Pseudomonas aeruginosa*, Protein Expr. Purif. 101 (2014) 138–145, https://doi.org/10.1016/j.pep.2014.06.012.
[41] A.T. Smith, A.E. Sestok, Expression and purification of functionally active ferrous iron transporter FeoB from Klebsiella pneumoniae, Protein Expr. Purif. 142 (2018) 1–7, https://doi.org/10.1016/j.pep.2017.09.007.
[42] B.C. Choy, R.J. Cater, F. Mancia, E.E. Pryor, Jr., A 10-year meta-analysis of membrane protein structural biology: detergents, membrane mimetics, and structure determination techniques, Biochim. Biophys. Acta Biomembr. 1863 (3) (2021) 183533, https://doi.org/10.1016/j.bbamem.2020.183533.
[43] K.N. Goldie, P. Abeyrathne, F. Kebbel, M. Chami, P. Ringler, H. Stahlberg, Cryo-electron microscopy of membrane proteins, Methods Mol. Biol. 1117 (2014) 325–341, https://doi.org/10.1007/978-1-62703-776-1_15.
[44] H.E. Autzen, D. Julius, Y. Cheng, Membrane mimetic systems in CryoEM: keeping membrane proteins in their native environment, Curr. Opin. Struct. Biol. 58 (2019) 259–268, https://doi.org/10.1016/j.sbi.2019.05.022.
[45] S. Li, Detergents and alternatives in cryo-EM studies of membrane proteins, Acta Biochim. Biophys. Sin. Shanghai 54 (8) (2022) 1049–1056, https://doi.org/10.3724/abbs.2022088.
[46] H.J. Lee .L.H.S., T. Youn, B. Byrne, P.S. Chae, Impact of novel detergents on membrane protein studies, Chem 8 (4) (2022) 980–1013, https://doi.org/10.1016/j.chempr.2022.02.007.
[47] T.H. Bayburt, Y.V. Grinkova, S.G. Sligar, Self-assembly of discoidal phospholipid bilayer nanoparticles with membrane scaffold proteins, Nano Lett. 2 (8) (2002) 853–856.
[48] T.H. Bayburt, Y.V. Grinkova, S.G. Sligar, Assembly of single bacteriorhodopsin trimers in bilayer nanodiscs, Arch. Biochem. Biophys. 450 (2) (2006) 215–222, https://doi.org/10.1016/j.abb.2006.03.013.
[49] J.W. Young, Recent advances in membrane mimetics for membrane protein research, Biochem. Soc. Trans. 51 (3) (2023) 1405–1416, https://doi.org/10.1042/BST20230164.
[50] T.J. Knowles, R. Finka, C. Smith, Y.P. Lin, T. Dafforn, M. Overduin, Membrane proteins solubilized intact in lipid containing nanoparticles bounded by styrene maleic acid copolymer, J. Am. Chem. Soc. 131 (22) (2009) 7484–7485, https://doi.org/10.1021/ja810046q.
[51] C. Sun, R.B. Gennis, Single-particle cryo-EM studies of transmembrane proteins in SMA copolymer nanodiscs, Chem. Phys. Lipids 221 (2019) 114–119, https://doi.org/10.1016/j.chemphyslip.2019.03.007.
[52] M. Parmar, S. Rawson, C.A. Scarff, A. Goldman, T.R. Dafforn, S.P. Muench, V.L. G. Postis, Using a SMALP platform to determine a sub-nm single particle cryo-EM membrane protein structure, Biochim. Biophys. Acta Biomembr. 1860 (2) (2018) 378–383, https://doi.org/10.1016/j.bbamem.2017.10.005.
[53] G.M. Di Mauro, N.Z. Hardin, A. Ramamoorthy, Lipid-nanodiscs formed by paramagnetic metal chelated polymer for fast NMR data acquisition, Biochim. Biophys. Acta Biomembr. 1862 (9) (2020) 183332, https://doi.org/10.1016/j.bbamem.2020.183332.
[54] G.J. Dodge, H.M. Bernstein, B. Imperiali, A generalizable protocol for expression and purification of membrane-bound bacterial phosphoglycosyl transferases in liponanoparticles, Protein Expr. Purif. 207 (2023) 106273, https://doi.org/10.1016/j.pep.2023.106273.
[55] J.M. Dorr, S. Scheidelaar, M.C. Koorengevel, J.J. Dominguez, M. Schafer, C.A. van Walree, J.A. Killian, The styrene-maleic acid copolymer: a versatile tool in membrane research, Eur. Biophys. J. 45 (1) (2016) 3–21, https://doi.org/10.1007/s00249-015-1093-y.
[56] J. Broecker, B.T. Eger, O.P. Ernst, Crystallogenesis of membrane proteins mediated by polymer-bounded lipid Nanodiscs, Structure 25 (2) (2017) 384–392, https://doi.org/10.1016/j.str.2016.12.004.
[57] J. Feng, Y. Chen, J. Pu, X. Yang, C. Zhang, S. Zhu, Y. Zhao, Y. Yuan, H. Yuan, F. Liao, An improved malachite green assay of phosphate: mechanism and application, Anal. Biochem. 409 (1) (2011) 144–149, https://doi.org/10.1016/j.ab.2010.10.025.
[58] C. Gomez-Garzon, S.M. Payne, Vibrio cholerae FeoB hydrolyzes ATP and GTP in vitro in the absence of stimulatory factors, Metallomics 12 (12) (2020) 2065–2074, https://doi.org/10.1039/d0mt00195c.
[59] M. Shin, A.R. Mey, S.M. Payne, FeoB contains a dual nucleotide-specific NTPase domain essential for ferrous iron uptake, Proc. Natl. Acad. Sci. USA 116 (10) (2019) 4599–4604, https://doi.org/10.1073/pnas.1817964116.
[60] A.P. Guilfoyle, C.N. Deshpande, K. Vincent, M.M. Pedroso, G. Schenk, M.J. Maher, M. Jormakka, Structural and functional analysis of a FeoB A143S G5 loop mutant explains the accelerated GDP release rate, FEBS J. 281 (9) (2014) 2254–2265, https://doi.org/10.1111/febs.12779.
[61] K.L. Hsueh, L.K. Yu, Y.H. Chen, Y.H. Cheng, Y.C. Hsieh, S.C. Ke, K.W. Hung, C. J. Chen, T.H. Huang, FeoC from Klebsiella pneumoniae contains a [4Fe-4S] cluster, J. Bacteriol. 195 (20) (2013) 4726–4734, https://doi.org/10.1128/JB.00687-13.
[62] M. Hattori, Y. Jin, H. Nishimasu, Y. Tanaka, M. Mochizuki, T. Uchiumi, R. Ishitani, K. Ito, O. Nureki, Structural basis of novel interactions between the small-GTPase and GDI-like domains in prokaryotic FeoB iron transporter, Structure 17 (10) (2009) 1345–1355, https://doi.org/10.1016/j.str.2009.08.007.
[63] A.E. Sestok, S.M. O'Sullivan, A.T. Smith, A general protocol for the expression and purification of the intact transmembrane transporter FeoB, Biochim. Biophys. Acta Biomembr. 1864 (9) (2022) 183973, https://doi.org/10.1016/j.bbamem.2022.183973.
[64] E. Reading, T.A. Walton, I. Liko, M.T. Marty, A. Laganowsky, D.C. Rees, C. V. Robinson, The effect of detergent, temperature, and lipid on the oligomeric state of MscL constructs: insights from mass spectrometry, Chem. Biol. 22 (5) (2015) 593–603, https://doi.org/10.1016/j.chembiol.2015.04.016.
[65] Y.C. Lee, J.A. Bååth, R.M. Bastle, S. Bhattacharjee, M.J. Cantoria, M. Dornan, E. Gamero-Estevez, L. Ford, L. Halova, J. Kernan, et al., Impact of detergents on membrane protein complex isolation, J. Proteome Res. 17 (1) (2018) 348–358, https://doi.org/10.1021/acs.jproteome.7b00599.
[66] V. Postis, S. Rawson, J.K. Mitchell, S.C. Lee, R.A. Parslow, T.R. Dafforn, S. A. Baldwin, S.P. Muench, The use of SMALPs as a novel membrane protein scaffold for structure study by negative stain electron microscopy, Biochim. Biophys. Acta 1848 (2) (2015) 496–501, https://doi.org/10.1016/j.bbamem.2014.10.018.
[67] A.C.K. Teo, S.C. Lee, N.L. Pollock, Z. Stroud, S. Hall, A. Thakker, A.R. Pitt, T. R. Dafforn, C.M. Spickett, D.I. Roper, Analysis of SMALP co-extracted phospholipids shows distinct membrane environments for three classes of bacterial membrane protein, Sci. Rep. 9 (1) (2019) 1813, https://doi.org/10.1038/s41598-018-37962-0.
[68] O.P. Hawkins, C.P.T. Jahromi, A.A. Gulamhussein, S. Nestorow, T. Bahra, C. Shelton, Q.K. Owusu-Mensah, N. Mohiddin, H. O'Rourke, M. Ajmal, et al., Membrane protein extraction and purification using partially-esterified SMA polymers, Biochim. Biophys. Acta Biomembr. 2021 (12) (1863) 183758, https://doi.org/10.1016/j.bbamem.2021.183758.
[69] S. Seyedmohammad, N.A. Fuentealba, R.A. Marriott, T.A. Goetze, J.M. Edwardson, N.P. Barrera, H. Venter, Structural model of FeoB, the iron transporter from *Pseudomonas aeruginosa*, predicts a cysteine lined, GTP-gated pore, Biosci. Rep. 36 (2) (2016), https://doi.org/10.1042/bsr20160046.
[70] B. Stevenson, E.E. Wyckoff, S.M. Payne, *Vibrio cholerae* FeoA, FeoB, and FeoC interact to form a complex, J. Bacteriol. 198 (7) (2016) 1160–1170, https://doi.org/10.1128/jb.00930-15.
[71] P.A. Lanzetta, L.J. Alvarez, P.S. Reinach, O.A. Candia, An improved assay for nanomole amounts of inorganic phosphate, Anal. Biochem. 100 (1) (1979) 95–97.